

# An impedance tube submerged in a liquid for the low-frequency transmission-loss measurement of a porous material

Miša Oblak<sup>a</sup>, Miha Pirnat<sup>a</sup>, Miha Boltežar<sup>b,\*</sup>

<sup>a</sup>*Kolektor Etra d.o.o., Šlandrova 10, 1231 Ljubljana, Slovenia*

<sup>b</sup>*Faculty of Mechanical Engineering, Aškerčeva 6, 1000 Ljubljana, Slovenia*

---

Cite as:

Miša Oblak, Miha Pirnat, Miha Boltežar  
An impedance tube submerged in a liquid for the low-frequency  
transmission-loss measurement of a porous material  
Applied Acoustics, Vol. 139, p. 203-212, 2018  
DOI: 10.1016/j.apacoust.2018.04.014

## Abstract

According to the standard ASTM E2611 an impedance tube can be used to measure the sound transmission and reflection losses in an absorption material. However, application in a liquid medium in the low-frequency range presents difficulties with respect to the size of the structure and the waveguide-related distortion of the plane-wave propagation. In this paper a four-microphone impedance tube for use in liquids in the low-frequency range, complying with the transfer-matrix method for transmission-loss measurements, is presented. The impedance tube is validated on the basis of research on an underwater, two-microphone impedance tube. It is demonstrated that in the low-frequency range the loudspeaker couples well into the plane-wave propagation. Furthermore, existing methods for measuring the group velocity and the complex wavenumber, applicable to the impedance tube, were investigated and compared to the new methods developed in this article. The results showed the best fits for the cross-correlation and the new approach of amplitude matching, respectively, for the cases of the velocity and the wavenumber measurements. Thus, the validated impedance tube was used for acoustic measurements of metal-foam samples. Problem-specific equations for calculating the dissipation coefficients of cavity-backed samples were derived from the transfer matrix and the scattering matrix. Stable results in agreement with the expected low absorption were obtained.

*Keywords:* impedance tube, metal foam, low frequency, waveguide,

---

\*Corresponding author. Tel.: +386 1 4771 608

*Email addresses:* [misa.oblak@kolektor.com](mailto:misa.oblak@kolektor.com) (Miša Oblak), [miha.pirnat@kolektor.com](mailto:miha.pirnat@kolektor.com) (Miha Pirnat), [miha.boltezar@fs.uni-lj.si](mailto:miha.boltezar@fs.uni-lj.si) (Miha Boltežar)

## 1. Introduction

For the effective use of absorption materials to dampen the noise in acoustic systems it is necessary to determine their ability to absorb sound energy. Wang [1] investigated the underwater sound-absorption properties of a porous metal impregnated with a viscous fluid, Sun and Hou [2] measured the sound absorption of a rubber material with an underwater pulse tube, and Xu *et al.* [3] studied the underwater performance of an air-saturated SiC foam and presented improvements in later work [4]. Impedance-tube-based methods, together with other standardized test methods, offer the possibility of absorption measurements in liquids. Implementation in the low-frequency range is particularly demanding, especially in the liquid environment. While the market offers commercial impedance-tube designs for use in a gaseous medium, the scope of use in liquids is to a large extent still unexplored. The fluid-structure interaction can distort the plane-wave propagation, which is the fundamental requirement for the impedance-tube measurement methods. Research on a water-filled impedance tube was conducted by Wilson *et al.* [5]. They investigated an impedance tube based on ASTM E1050 [6], which is a two-microphone method with a rigidly backed sample. Their work was concentrated on the pressure sensor's design, an analysis of waveguide effects and the corresponding restrictions due to the wavefront curvature and the dispersion of the sound velocity.

Porous materials, like metal foams, have inferior absorption properties in the low-frequency range, especially when backed by a rigid plate, as reported by Han *et al.* [7] and Navacerrada *et al.* [8]. Therefore, measurements based on the two-microphone impedance-tube design cannot provide useful results. Furthermore, the two-microphone method does not permit transmission-loss measurements, as only reflection can be observed. Accordingly, the four-microphone method for a normal incidence, sound-transmission measurement with a cavity-backed sample, as stated in ASTM E2611 [9], is more appropriate for this application.

Several methods for the evaluation of acoustic properties using a four-microphone impedance tube can be found in literature. The standard ASTM E2611 [9] specifies the transfer-matrix method by Song and Bolton [10]. The transfer matrix correlates the sound pressure and the particle velocity on each side of the sample, and can be freely multiplied to evaluate the characteristics of multiple absorption layers in series. The reflection and the transmission coefficient are presented implicitly with four elements of the transfer matrix. Similarly, the scattering-matrix method presented by Åbom [11] correlates the pressure amplitudes of the incident and reflected waves using the reflection and transmission coefficients. The procedure for extracting the scattering-matrix elements is analogous to the transfer-matrix method. Due to the explicitly written coefficients it is convenient for analysing a single layer of the test sample, but a transfer-matrix implementation is required for a further study of multiple layers, as reported

by Feng [12]. In addition, Salissou and Penneton [13] revised the wave-field decomposition method from Ho *et al.* [14] to avoid the corresponding assumptions of sample symmetry. Like with the scattering matrix, the reflection coefficients for both directions of the wave propagation and the transmission coefficient are obtained explicitly, again causing a limitation with respect to the use for a measured layer of porous material. The previously mentioned methods are all two-load methods, requiring measurements of two different boundary conditions of the wave termination. However, this is not the case for the method described by Bonfiglio and Pompoli [15], who combined the transfer matrix and wave-field decomposition into a single measurement approach. Salissou and Penneton [13] observed that the results of a single measurement approach match with the two-load methods, but only when the acoustic load is relatively absorbing. Looking at the presented methods, the transfer-matrix method is the only one to characterize the general material-absorption properties with ease of use for multiple layers and different impedance-tube configurations.

The objective of this paper is to develop a four-microphone impedance tube for low-frequency sound-absorption measurements in liquid media. Although the standard ASTM E2611 [9] specifies a recommended design for the four-microphone impedance tube, it is mainly intended for use in gaseous media. No appropriate design for such a tube submerged in liquid was reported in the literature. Therefore, based on an underwater impedance tube, a new four-microphone instrument was developed, specifically for transmission-loss measurements in a liquid medium in the frequency range 70-560 Hz. For reasons of practicality, the transfer-matrix method is employed to evaluate the absorption properties. The calculation of the problem-specific absorption of a cavity-backed configuration under study in this paper requires a new approach for the reflection and transmission coefficients. This new approach consists of equations for sound absorption, obtained using a correlation of the transfer matrix [10] and the scattering matrix [12].

The pivotal acoustic parameters for the transmission-loss calculation include the sound velocity and the complex wavenumber; therefore, it is best to measure them on-site. For the case of the group sound velocity two new methods based on the first mode of an open-end column and the cross-correlation are introduced and compared to the basic method of the signal travel time and the minimum-difference method adapted from the work of Wang *et al.* [16]. For the case of the wavenumber, both numerical and analytical solutions are available. The latter was adapted from Wilson *et al.* [5]. On the other hand, the numerical evaluation of the wavenumber with the established methods of Peters *et al.* [17], Hou *et al.* [18] and Han *et al.* [19] did not produce valid results. For the needs of the new approach, amplitude-matching method is developed.

In Section 2 a short overview of the transfer-matrix method is followed by a derivation of the coefficients for the cavity-backed configuration. The design of the developed impedance tube is described and the operation of the experimental setup is explained. For the purposes of the impedance tube's validation (Section 3) a further investigation of the acoustic phenomena, such as the tube attenuation and the waveguide effect, is performed. This includes an overview

of the methods for the measurements of the group sound velocity and the complex wavenumber. Finally, a validated impedance tube is used for the acoustic testing of the open-porous metal-foam samples, as presented in Section 4, and the corresponding results are discussed in Section 5.

## 2. Transfer matrix method

The impedance tube based on the transfer-matrix method is presented in the standard ASTM E2611 [9]. It is designed to measure the change in the pressure field with a four-point measuring system and extract the acoustic absorption. A simplified model of such a measuring system is shown in Fig. 1. The sound waves are excited with a transducer on the left-hand side of the tube and the waves, transmitted to the other side, are met with the boundary condition in the form of an acoustic load. The sample of the absorption material divides the propagated waves into two different pressure fields and the corresponding amplitudes of the incident ( $A$  and  $C$ ) and outbound waves ( $B$  and  $D$ ):

$$p(x < 0) = A e^{-j k x} + B e^{+j k x}, \quad (1)$$

$$p(x > d) = C e^{-j k x} + D e^{+j k x}, \quad (2)$$

where  $d$  is the sample thickness and the wavenumber  $k = k_r - j k_i$  is a complex number, with  $j$  being the imaginary unit. The real component  $k_r = \frac{\omega}{c}$  describes the ratio of the angular frequency  $\omega$  and the sound velocity  $c$ . The imaginary component  $k_i$  represents the attenuation constant, which includes the viscosity and the thermal dissipation in the tube.

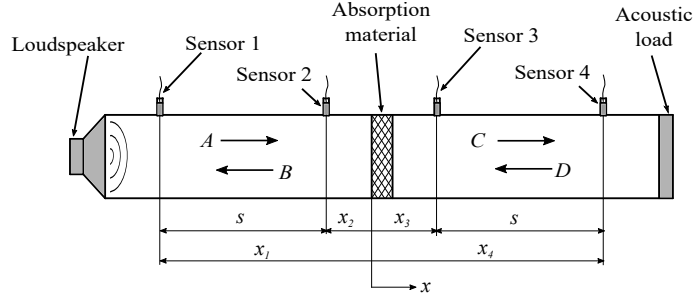


Figure 1: Impedance tube based on ASTM E2611.

The pressure amplitudes are calculated from the transfer functions  $H_{n,\text{ref}}$

measured at the position of the sensors with the numbers  $n = 1, 2, 3, 4$  [9]:

$$A = j \frac{H_{1,\text{ref}} e^{+j k x_2} - H_{2,\text{ref}} e^{+j k x_1}}{2 \sin [k (x_1 - x_2)]}, \quad (3)$$

$$B = j \frac{H_{2,\text{ref}} e^{-j k x_1} - H_{1,\text{ref}} e^{-j k x_2}}{2 \sin [k (x_1 - x_2)]}, \quad (4)$$

$$C = j \frac{H_{3,\text{ref}} e^{+j k x_4} - H_{4,\text{ref}} e^{+j k x_3}}{2 \sin [k (x_3 - x_4)]}, \quad (5)$$

$$D = j \frac{H_{4,\text{ref}} e^{-j k x_3} - H_{3,\text{ref}} e^{-j k x_4}}{2 \sin [k (x_3 - x_4)]}. \quad (6)$$

The amplitudes obtained with Eq. (3)-(6) are used for the derivation of the transfer-matrix elements, as described in ASTM E2611 [9]. The transfer matrix relates the acoustic pressure  $p$  and the particle velocity  $u$  on each side of the sample:

$$\begin{bmatrix} p_1 & p_2 \\ u_1 & u_2 \end{bmatrix}_{x=0} = \begin{bmatrix} T_{11} & T_{12} \\ T_{21} & T_{22} \end{bmatrix} \begin{bmatrix} p_1 & p_2 \\ u_1 & u_2 \end{bmatrix}_{x=d}, \quad (7)$$

where the indices 1 and 2 mark two different acoustic loads: the partially anechoic and the rigid termination. In this way no assumptions are made regarding the sample symmetry. On the basis of the transfer matrix, the transmission coefficient  $t$  and the reflection coefficient  $r$  can be predicted for multiple tube termination configurations and the corresponding transmission loss  $TL_n$  and the absorption coefficient  $\alpha$  can be calculated using the following equations:

$$TL_n = 20 \log_{10} \left| \frac{1}{t} \right|, \quad (8)$$

$$\alpha = 1 - |r|^2 - |t|^2. \quad (9)$$

Song and Bolton [10] offered solutions for the anechoic termination:

$$t_{\text{anech}} = \frac{2 e^{j k d}}{T_{11} + \frac{T_{12}}{\rho c} + \rho c T_{21} + T_{22}}, \quad (10)$$

$$r_{\text{anech}} = \frac{T_{11} + \frac{T_{12}}{\rho c} - \rho c T_{21} - T_{22}}{T_{11} + \frac{T_{12}}{\rho c} + \rho c T_{21} + T_{22}}, \quad (11)$$

and the rigid termination, where the sample is backed by a rigid plate:

$$t_{\text{rigid}} = 0, \quad (12)$$

$$r_{\text{rigid}} = \frac{T_{11} - \rho c T_{21}}{T_{11} + \rho c T_{21}}. \quad (13)$$

Han *et al.* [7] and Navacerrada *et al.* [8] observed that dissipation in the low-frequency range improves when the absorption material is backed by a cavity. Therefore, the absorption of the sample in the cavity-backed configuration is of interest. In this paper problem-specific equations are obtained with the correlation of the transfer matrix and the scattering matrix.

### 2.1. Cavity-backed formulation

The transfer matrix, although representing a general material property, does not offer a straightforward solution for the absorption coefficient in the cavity-backed configuration. The scattering matrix, as presented in the work of Feng [12], is easier to employ. At this point it must be emphasized that with a presupposed unsymmetrical sample, we have two different reflection coefficients  $r_{AB}$  and  $r_{DC}$ . The first one describing the reflection from the sample towards the loudspeaker and second one the reflection from the sample towards the tube's termination. As identified by Salissou *et al.* [13], even for symmetrical samples, the assumption of  $r_{AB} = r_{DC}$  is too restrictive, as the boundary conditions on the upstream and downstream sides of the sample are generally different. Considering the acoustic loads 1 and 2, the scattering matrix couples the pressure-field amplitudes in the following way [12]:

$$\begin{bmatrix} B_1 & B_2 \\ C_1 & C_2 \end{bmatrix} = \begin{bmatrix} r_{AB} & t_{DB} \\ t_{AC} & r_{DC} \end{bmatrix} \begin{bmatrix} A_1 & A_2 \\ D_1 & D_2 \end{bmatrix}. \quad (14)$$

Based on the scattering-matrix elements Feng [12] obtained the dissipation for the configuration of the cavity with a rigid termination:

$$r_{\text{cavity}} = r_{AB} + \frac{t^2 e^{-2jkx_t}}{1 - r_{DC} e^{-2jkx_t}}, \quad (15)$$

where  $x_t$  represents the location of the termination plate in the impedance tube's coordinate system. In contrast to the reflection, the transmission coefficient  $t$  for both sides of the sample can be unified on the basis of the reciprocity principle [10], yielding  $t = t_{AC} = t_{DB}$ . The corresponding transmission loss for the single transition of the wave through the absorption material can be obtained by inserting  $t$  into Eq. 8. Since the dissipation between the tube's input and output sound waves is of interest, the transmission loss is already incorporated into  $r_{\text{cavity}}$ , making  $\alpha_{\text{cavity}} = 1 - |r_{\text{cavity}}|^2$ .

Assuming that the transfer-matrix elements are known, they can be used to obtain the absorption coefficient for the cavity-backed sample on the basis of Eq. 15. Beforehand, the correlation between the scattering matrix, meaning the unknown coefficients  $r_{AB}$ ,  $r_{DC}$  and  $t$ , and the transfer matrix, must be derived. This is based on observing the unit input wave in two different load configurations, i.e., the rigid and anechoic termination. This accounts for  $A_1 = 1$ ,  $D_1 = C e^{-2jkx_t}$  for the first and  $A_2 = 1$ ,  $D_2 = 0$  for the second case. Inserting these amplitudes into Eq. 14, the corresponding amplitudes  $B$  and  $C$  for each load can be obtained. The amplitudes are thus defined as a function of  $r_{AB}$ ,  $r_{DC}$  and  $t$ , and can be used to evaluate the pressure and velocity on the

front and back surfaces of the sample:

$$p_i(x=0) = A_i + B_i, \quad (16)$$

$$u_i(x=0) = \frac{A_i - B_i}{\rho c}, \quad (17)$$

$$p_i(x=d) = C_i e^{-jkd} + D_i e^{jkd}, \quad (18)$$

$$u_i(x=d) = \frac{C_i e^{-jkd} - D_i e^{jkd}}{\rho c}, \quad (19)$$

where  $i$  represents load case 1 or 2. Inserting the evaluated pressures and velocities into Eq. 7 and solving for the coefficients yields:

$$r_{AB} = \frac{T_{11} + \frac{1}{\rho c} T_{12} - \rho c T_{21} - T_{22}}{T_{11} + \frac{1}{\rho c} T_{12} + \rho c T_{21} + T_{22}}, \quad (20)$$

$$r_{DC} = e^{2jkd} \frac{-T_{11} + \frac{1}{\rho c} T_{12} - \rho c T_{21} + T_{22}}{T_{11} + \frac{1}{\rho c} T_{12} + \rho c T_{21} + T_{22}}, \quad (21)$$

$$t_{AC} = 2e^{jkd} \frac{1}{T_{11} + \frac{1}{\rho c} T_{12} + \rho c T_{21} + T_{22}}, \quad (22)$$

$$t_{DB} = 2e^{jkd} \frac{T_{11} T_{22} - T_{12} T_{21}}{T_{11} + \frac{1}{\rho c} T_{12} + \rho c T_{21} + T_{22}}, \quad (23)$$

where  $T_{12} T_{21} - T_{11} T_{22} = 1$  and consequently  $t_{AC} = t_{DB}$ , on the basis of the reciprocity principle. Finally, the coefficients can be inserted into Eq. 15 for the calculation of the absorption coefficient. Thus, combining the transfer and scattering matrices we derived a formulation for the dissipation parameters in the cavity-backed configuration. The stated formulation will be used to analyse the results of the measurements on the metal foams presented in this paper. It is understandable that the accuracy of the measured transfer functions  $H_{n,\text{ref}}$  and therefore the calculated transfer-matrix elements and the dissipation coefficients depend on the design of the impedance tube.

## 2.2. Impedance tube

The instrument design for the low-frequency impedance tube submerged in a liquid is subjected to problem-specific construction requirements. In particular, the distance between the sensors is associated with the accuracy of the measurements. As reported by Bodén and Åbom [20] the transfer functions are the least sensitive to external interferences when the distance between the sensors  $s$  equals a quarter of a wavelength. Peng *et al.* [21] further investigated the fact that an error of the same extent can be guaranteed in the interval  $0.05c < fs < 0.4c$ , with ASTM E2611 [9] expanding the lower limit to  $0.01c < fs < 0.4c$ .

A standardized impedance tube must also fulfil the assumption of a plane-wave distribution, which might become distorted in a liquid-immersed tube due to the fluid-structure interaction. The sound pressure excites the elastic waves in the tube wall, which are accompanied by radial particle oscillation

and wavefront curvature. In order to avoid the distortion of the plane waves the tube wall must be acoustically rigid. Del Grosso [22] and Baik *et al.* [23] studied the axial wave propagation within liquid-filled cylinders with elastic walls of finite thickness in order to obtain the characteristic equation for axisymmetric modes. Del Grosso [22] reported that a less than 1 % dispersion in the fundamental mode can be achieved with a wall thickness approaching the value of inner tube radius. Wilson *et al.* [5] further observed, based on measurements in a water-filled impedance tube, that the deviation between the pressure in the tube axis and the pressure at the wall does not exceed 1 % in the low-frequency range of the fundamental mode.

The designed impedance tube is shown in Fig. 2. It represents a thick-walled structural steel tube of inner diameter 79 mm, wall thickness 40 mm and length 3 m. The distance between the sensor  $s = 1$  m limits the usable frequency range to 70-560 Hz. The steel's rigidity was maintained by fabricating the tube entirely from one piece. Additional flanges on each side of tube enable the mounting of a loudspeaker and a 40-mm-thick termination plate.

### 2.3. Experimental setup

The measurement scheme for the impedance-tube test station is presented in Fig. 2. For the purposes of easy handling of the samples, the entire assembly was submerged into the liquid medium, i.e., Nynas Nytro 10XN transformer oil. The pulse signal, generated in the LabVIEW programming environment, was applied to the system as an excitation signal. Using the NI 9263 module and a Renkforce PA MP-2000 RMS amplifier, the signal was transmitted to a DNH Aqua-30 loudspeaker with a uniform power distribution over a frequency of 90 Hz. The pressure response was obtained with hermetically sealed PCB 106B52 pressure sensors at four measuring points along the tube. The sensors have a steel membrane to enforce the tube's rigidity and provide a high mechanical input impedance; therefore, avoiding the perturbation of the pressure field. The signals were transferred to the computer by the NI 9234 module for further post-processing. The oil temperature was monitored with a resistance thermometer (RTD) through the NI 9219 input module.

The impedance tube was backed by a thick plate, which was fixed onto the tube flange in the case of a rigid termination. For the second load configuration, which is a partially anechoic termination, the plate was translated in the axial direction to create a decompression slot  $\delta = 5$  mm (Fig. 2).

## 3. Acoustic phenomena in impedance tube

Acoustic phenomena, such as the wavefront curvature, the sound attenuation and the dispersion of the sound velocity, can be observed in acoustic waves propagating through cylinders due to the fluid-structure interaction. Before conducting the experiment we ensured that the measurement system conforms to the condition of a plane-wave distribution and calculated any unknown sound velocity and dissipation characteristics of the transformer oil. The wave number, and consequently the sound velocity itself, is a fundamental parameter in

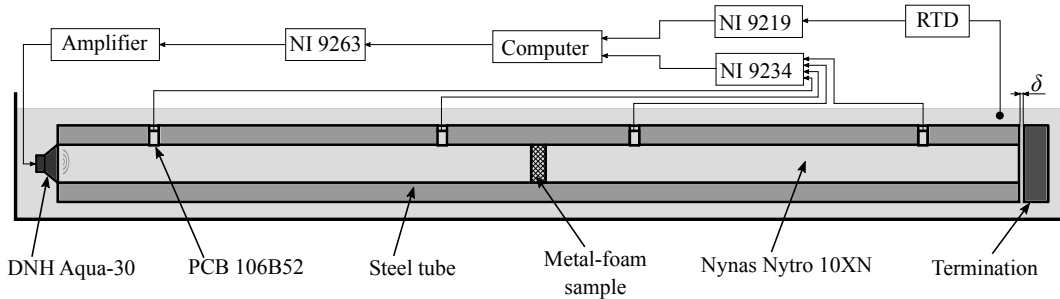


Figure 2: Experimental setup with the impedance tube submerged in transformer oil. Excitation, pressure and temperature signals are monitored using the output module NI 9263 and the input modules NI 9234 and NI 9219, respectively. Different load configurations can be achieved with the decompression slot  $\delta$ .

the derivation of the pressure-field amplitudes. As such data is not specified for transformer oil, it needs to be determined with an experiment.

Transformer oil is a dispersive medium; therefore, the frequency-dependent phase velocity  $c_0$ , defined as the real component of  $\frac{\omega}{k}$ , can be detected. On the other hand, the group velocity  $c_1$ , meaning the velocity at which the pulse signal is propagated in the medium, is also of interest, especially for a theoretical formulation of the tube attenuation and an investigation of the waveguide effects. The latter is required to show that in the low-frequency range for a given tube design no problems with a disruption of plane-wave propagation arise.

### 3.1. Group sound velocity

The group sound velocity can be easily deduced from measured pressure signals in either the time or frequency domain. Four methods were tested, which can be implemented without any further changes to the existing measurement system. These methods include an open-end column natural modes analysis, a manual extraction of the time difference between the signals, a cross-correlation of the signals and the minimum difference between the frequencies.

The first approach is the frequency-domain method based on the natural modes of the open-end column. It is the only exception to using standard measurements, as the loudspeaker needs to be decoupled from the impedance tube to provide the appropriate boundary condition. The fluid inside the tube is excited from a distance and thus the first natural frequency  $f_1$  of the open-end column can be obtained, followed by the velocity  $c_1 = 4(l + l') f_1$ , where  $l$  is the tube's length and  $l'$  is the tube's end correction. The latter is used to compensate for the actual acoustic length, which is greater than the physical length due to radiation. The end correction in the form of  $l' = 0.8r$  can be used for the case of an infinitely flanged rigid-walled cylinder, as reported by Silva *et al.* [24] and Ogawa *et al.* [25]. The equivalent formula can be applied for higher harmonics (odd multiples). The resultant velocity depends on the accuracy of the open-end condition; therefore, the procedure was repeated while increasing the distance between the tube flange and the loudspeaker diaphragm  $h$  until the

$c_1$  value converged at  $h = 40$  mm. Fig. 3 shows the results in comparison with other methods.

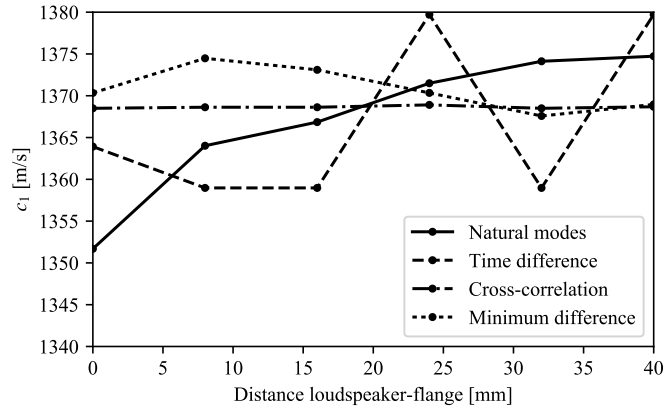


Figure 3: Comparison of different methods for the group sound-velocity determination as a function of the loudspeaker-flange distance.

The time-difference method is a calculation of the amount of time the impulse signal needs to travel the distance between two sensors. One such response measurement is presented in Fig. 4. It is recommended to use a high sampling frequency, otherwise it is hard to evaluate the exact time for the signal reaching the sensor's position. Specifically, signals were sampled with a frequency of 25.6 kHz, and the results deviate by as much as 20 m/s (Fig. 3).

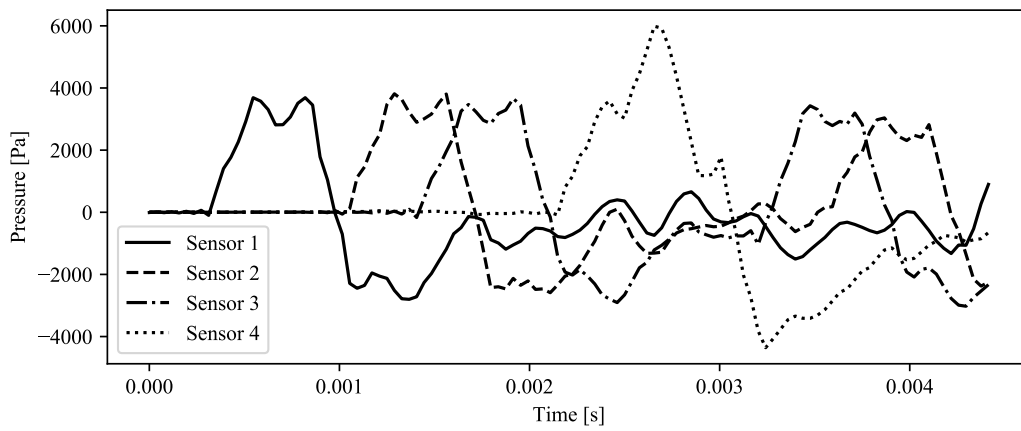


Figure 4: Pressure signals measured using sensors at the corresponding location. Increased pressure amplitude at sensor 4 is caused by the coinciding incident and reflected wave due to the proximity of the tube termination.

The next method is based on comparing two signals with a cross-correlation

analysis. The correlation function is calculated according to the formula  $\int_0^{t_{\max}} p_1(t) p_2(t + \tau) dt$ , where  $p_1$  and  $p_2$  are the pressure signals at positions 1 and 2, respectively. The time of the correlation function peak corresponds to the travelling time of the signal between the specified positions. The peak of the function is clearly defined (Fig. 5), even though the signals are somewhat distorted due to the medium’s dispersivity. Only the wave propagating toward the tube termination before the onset of the reflection can be taken into account. With regard to the Fig. 4 time of the wave reflection can be approximated at about 0.00245 s, that is before reflection related increased pressure amplitude at location of the sensor 4. Therefore only signals up to 0.00245 s from sensors 1, 2 and 3 can be used with cross-correlation method. The accuracy of the approximated time of the signal reflection is not crucial. Fig. 3 shows that this method gives more accurate results than the previous two. On the other hand, it requires a specific selection of the signal’s time interval.

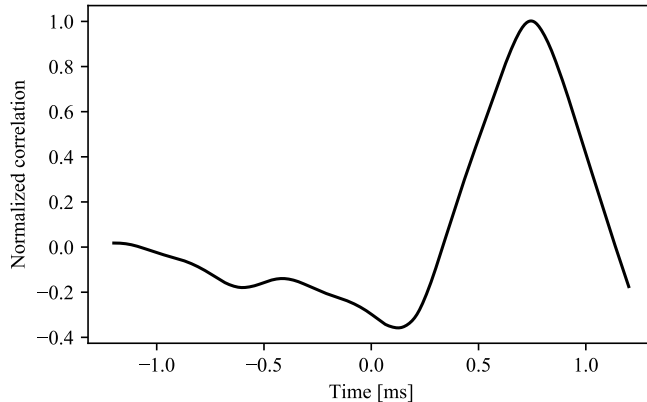


Figure 5: Cross-correlation function of the signals obtained with sensors 1 and 2.

The final group-velocity-measurement method is the minimum-frequencies-difference method, adapted from the work of Wang *et al.* [16]. The velocity is calculated using equation  $c_1 = 2 l_1 \Delta f$ , where  $l_1$  is the distance between the first sensor and the tube termination. The parameter  $\Delta f$  represents the frequency difference between two successive minima of the pressure amplitudes’ ratio  $\log \left| \frac{P_1}{P_2} \right|$ , with  $P_1$  being the Fourier transform of the pressure from the first sensor and  $P_2$  from the second sensor. Thus, the acquired velocity has a value similar to the cross-correlation method, but is not completely independent of the loudspeaker’s boundary condition, as seen in Fig. 3.

Overall, the cross-correlation method proved to be the most accurate with respect to the variable location of the loudspeaker and is used in our further analysis. Specifically for the transformer oil, the group velocity is 1369 m/s at 25.4°C. During the analysis the sensor positions were assumed to be fixed at physical positions. This does not necessarily coincide with the acoustic center

of the sensors [26], but for large wavelengths the deviations are negligible.

### 3.2. Waveguide effects

Under the influence of the waveguide dynamics, fundamental and higher modes are excited in the tube. Following the notation of Del Grosso [22], the axi-symmetric modes in the tube with elastic walls of finite thickness are denoted  $ETm$ , where  $m$  refers to the mode order. The fundamental mode  $ET0$  has a nearly plane wavefront and causes little dispersion and radial particle motion. In contrast, the next mode  $ET1$  has a more pronounced wavefront curvature and more radial displacement [5]. The transfer-matrix method requires plane-wave propagation; therefore,  $ET1$  and higher modes should not be generated. To check whether the loudspeaker is an appropriate excitation mechanism and the tube wall is sufficiently rigid, the speed-of-sound dispersion was analysed. Each individual mode  $m$  has a corresponding phase velocity  $c_{0m}$ , which can be obtained with the characteristic equation of Del Grosso [22] or Baik *et al.* [23]. The problem-specific parameters used to solve the characteristic equation are detailed in Tab. 1 and the results are shown in Fig. 6. The latter confirms that both  $ET0$  and  $ET1$  reach to the low frequency range.

Table 1: Material parameters of the liquid medium and the solid wall for the waveguide’s decomposition: inner tube radius  $b$ , outer tube radius  $d$ , transformer-oil density  $\rho_l$ , steel density  $\rho_w$ , group sound velocity  $c_l$ , longitudinal and shear sound velocity in steel  $c_l$  and  $c_s$ , respectively.

Transformer oil	Steel tube
$b = 39.5 \text{ mm}$	$\rho_w = 7850 \text{ kg/m}^3$
$d = 79.5 \text{ mm}$	$c_l = 5960 \text{ m/s}$
$\rho_l = 855.76 \text{ kg/m}^3$	$c_s = 3235 \text{ m/s}$
$c_l = 1369 \text{ m/s}$	

In order to prevent  $ET1$  excitation, the mismatch between the sound source wave’s propagation and the  $ET1$  modal shape must be provided. Although the back-enclosed speaker can be considered to have an acoustic response similar to a monopole with spherical wave propagation, no separated wavefronts with different sound velocities, as reported by Lafleur and Shields [27], could be observed from our measurements. Providing that mode  $ET1$  was in fact excited, its amplitude is negligible. Furthermore, in the frequency region of interest both the axial and radial particle displacements of  $ET1$  (Fig. 7), although larger than that of  $ET0$ , are much less problematic than reported for higher frequencies [23]. As shown in Fig. 7 the particle-displacement dispersion in  $ET1$  does not exceed a value of 0.01 in the axial direction and 0.2 in the radial direction at 560 Hz, which is the highest frequency in the range of interest. On the contrary, a ten-times-higher frequency means multiple times higher radial dispersion and an even more significant axial dispersion.

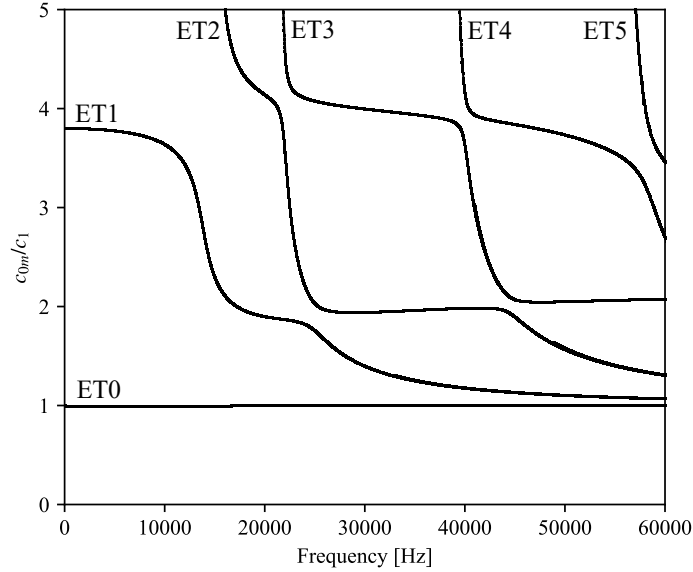


Figure 6: Normalized phase velocity for axi-symmetric modes ET0–ET5. With a higher frequency the  $c_{0m}$  of all the modes converges to  $c_1$  making the tube dynamics independent of the wall thickness.

### 3.3. Tube attenuation

Viscosity losses, thermal dissipation mechanisms and molecular relaxation cause an exponential decrease in the pressure amplitude throughout the wave propagation. This phenomenon is called attenuation. In an air-filled impedance tube the attenuation-related dissipation can be neglected due to relatively small distances between the sensors and consequently the overall more compact size of the tube. In contrast, the wavelengths in the liquid medium are many times longer, requiring larger tube dimensions. Since the metal-foam samples are expected to have a low absorption capacity [7, 3] all the possible dissipation mechanisms that might influence the results must be considered.

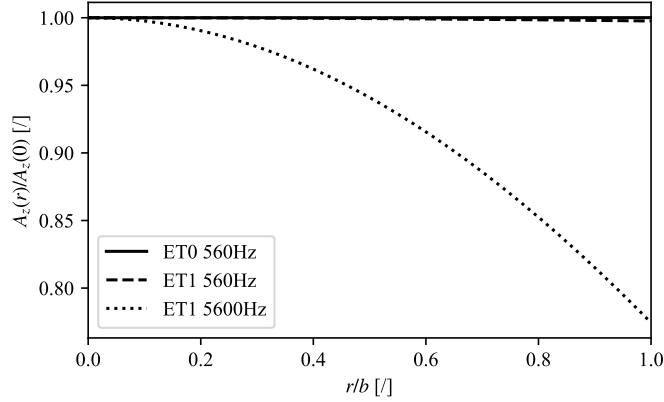
Attenuation is characterized by an imaginary component of the complex wavenumber  $k_i$ . The real component  $k_r$  corresponds to the frequency-dependent phase velocity  $c_0$ . For the case of the underwater impedance tube, Wilson *et al.* [5] approximated the complex wavenumber using the following equation:

$$k = \frac{\omega}{c_1} + (1 - j) \alpha_w, \quad (24)$$

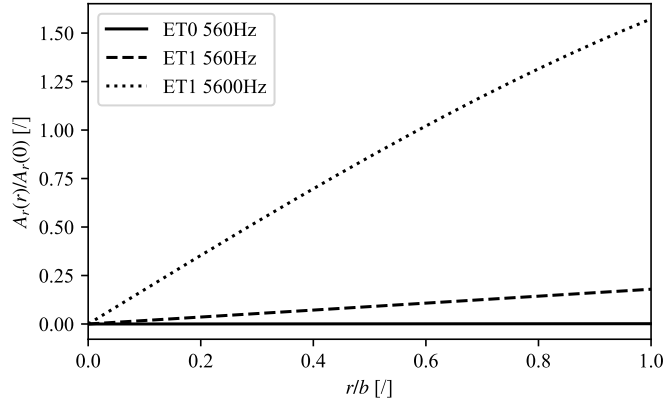
where  $\alpha_w$  represents the viscous losses in the fluid-structure interaction layer at the tube wall with inner radius  $b$ :

$$\alpha_w = \frac{1}{b} \sqrt{\frac{\mu \omega}{2 \rho c_1^2}}, \quad (25)$$

with  $\mu$  being dynamic viscosity of fluid. In this analytical formulation the bulk fluid losses are neglected, as are the thermal losses in the visco-thermal wall



(a)



(b)

Figure 7: Comparison of the normalized radial profile of the particle displacements for modes ET0 and ET1 at 560 Hz, and ET1 at 5000 Hz, obtained according to the definition by Lafleur and Shields [27]. The abscissa represents the radial position  $r$  normalized by the inner-tube radius  $b$ , and the ordinate represents the circumference-to-center ratio of the particle displacement, where  $A_z$  is the amplitude of the axial displacement and  $A_r$  is the amplitude of the radial displacement; a) Axial particle displacement normalized amplitude, b) Radial particle displacement normalized amplitude.

layer. Additionally, the equation assumes a small phase shift of the wavenumber  $\frac{\omega}{c_1} \gg \alpha_w$ . Furthermore, the effects of wall roughness, local discontinuities in geometry and potential oil impurities cannot be predicted with an analytical equation. Therefore, it is more reliable to measure the tube's attenuation constant.

Multiple methods for the numerical evaluation of the tube attenuation from impedance tube measurements can be found in the literature, including Peters *et al.* [17], Hou *et al.* [18] and Han *et al.* [19]. Peters and Petit [17] further developed

the cross-correlation analysis mentioned in Section 3.1 to include the phase shift and extract the phase velocity, mainly for ultrasound. It requires a measurement of the pulse signal without any reflection and a spectral analysis of the measured response. When implementing this method in an impedance tube only the time signals before the excitation pulse reaching the tube termination were taken into account and then padded with zeros in order to keep the frequency resolution of 0.5 Hz. The attenuation coefficient and the phase velocity for sensors  $n$  and  $n + 1$  are then defined as [17]:

$$k_i(f) = -\frac{\log \left| \frac{P_{n+1}(f)}{P_n(f)} \right|}{|x_{n+1} - x_n|}, \quad (26)$$

$$c_0(f) = -\frac{2\pi f |x_{n+1} - x_n|}{\text{Arg} \left( \frac{P_{n+1}(f) e^{2j\pi f \tau}}{P_n(f)} \right) - 2\pi f \tau}, \quad (27)$$

with  $P_n$  representing the Fourier transform of the pressure signal from the sensor  $n$  and  $x_n$  marking its position. The resultant values are evident from Fig. 8.

A basic iterative method for attenuation determination using a four-microphone tube is presented in the work of Hou and Bolton [18]. They used the measurement of an empty impedance tube, modelling the partial tube dissipation between sensors 2 and 3 as an absorption material. Implementing the standard transfer matrix and the equation for the propagation wavenumber in material  $k' = \frac{1}{d} \cos^{-1} T_{11}$  [9] into an iterative algorithm, the output  $k'$  was substituted into input  $k$  until the values converged. Although the method is straightforward the solution depends on the assumed material thickness and it leads to particularly unsteady results in our case, without any detectable trend.

Another numerical evaluation of the attenuation was presented by Han *et al.* [19]. The attenuation coefficient was obtained by closing the tube with a rigid termination, measuring the transfer function and comparing it to the theoretical value using the two-microphone method [6]. This is based on the assumption that rigid termination results in total reflection  $r = 1$ , which is very difficult to provide in liquids. Even though our own impedance-tube design includes a thick back plate with the appropriate sealing, an infinite impedance was not achieved.

Purposely excluding the rigid boundary condition from the wavenumber determination process, we concentrated on the pressure amplitudes  $A$ ,  $B$ ,  $C$  and  $D$ , with the first pair defining the upstream pressure field and the second pair the downstream field (Fig. 1). Providing the impedance tube is empty, meaning without any absorption material in between sensor 2 and 3, single pressure field can be observed inside the tube. Therefore, the pressure amplitude  $A$  of an incident wave, measured with sensors 1 and 2, should be equal to the pressure amplitude  $C$  of the same incident wave, measured with sensors 3 and 4. This also applies analogously to the pressure amplitudes of a reflected wave, namely

amplitudes  $B$  and  $D$ . Implementing Eq. (3)-(6) it follows that:

$$\frac{H_{1,\text{ref}} e^{+jkx_2} - H_{2,\text{ref}} e^{+jkx_1}}{2 \sin[k(x_1 - x_2)]} = \frac{H_{3,\text{ref}} e^{+jkx_4} - H_{4,\text{ref}} e^{+jkx_3}}{2 \sin[k(x_3 - x_4)]}, \quad (28)$$

$$\frac{H_{2,\text{ref}} e^{-jkx_1} - H_{1,\text{ref}} e^{-jkx_2}}{2 \sin[k(x_1 - x_2)]} = \frac{H_{4,\text{ref}} e^{-jkx_3} - H_{3,\text{ref}} e^{-jkx_4}}{2 \sin[k(x_3 - x_4)]}. \quad (29)$$

Numerically solving for  $k_r$  and  $k_i$ , the results shown in Fig. 8 were obtained. In comparison to other methods it can be observed that the measurement fits well with the analytical equation of Wilson *et al.* [5] for the case of the attenuation constant, with a mean absolute difference of 0.00468 Np/m since the analytical solution underestimates the dissipation. In contrast, implementation of the method by Peters *et al.* [17] was not successful. Both plots by Peters also have a reverse gradient compared to the others and depend on the chosen length of the time signal.

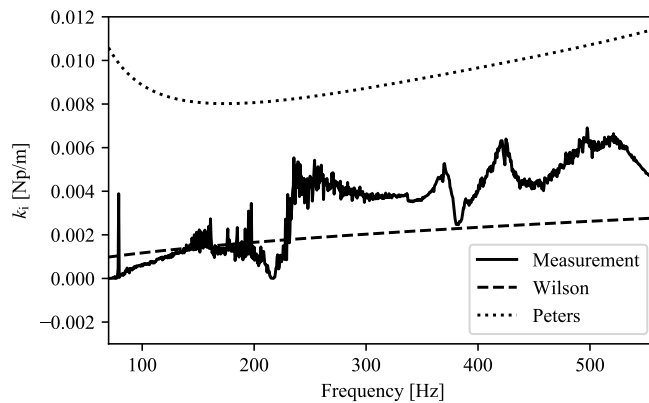
In the lower frequency range up to 90 Hz the measured wavenumber inconsistencies are due to the speaker's non-uniform power, especially under the pressure of the loudspeaker-tube coupling. Comparing the result to  $c_{00}$  by ET0 (Fig. 6) it is clear that the measurements show a significant difference between the group and the phase velocity. This is due to the fact that in Fig. 6 the viscosity and the thermal losses are neglected, as is the damping associated with radiation into the tube's surrounding liquid.

Fig. 8 shows a zero value of the measured attenuation constant and the corresponding fluctuation of the phase velocity at 216 Hz. This phenomenon coincides with the symmetrical mode presented in Fig. 9, where the loudspeaker and the termination plate excite the fluid in such a way that the monopolar resonance displacement is formed, as presented by Yang *et al.* [28]. The equivalent would be a tube with two pistons on each side, exciting the fluid in anti-phase. The distinct shape of phase velocity curve (Fig. 8b) is equal to that of the real component of complex effective mass in the vicinity of monopolar resonance, obtained by Yang *et al.* [28]. In monopolar mode of pressure the fluid volume oscillates, while the center of mass remains fixed, causing zero value of the real components of both effective bulk modulus  $\bar{K}$  and effective mass density  $\bar{\rho}$ . Consequently, the effective wavenumber  $\bar{k} = \omega \sqrt{\frac{\bar{\rho}}{\bar{K}}}$  becomes fully real, while imaginary component of the wavenumber becomes null. This becomes apparent in form of the attenuation constant with zero value at 216 Hz.

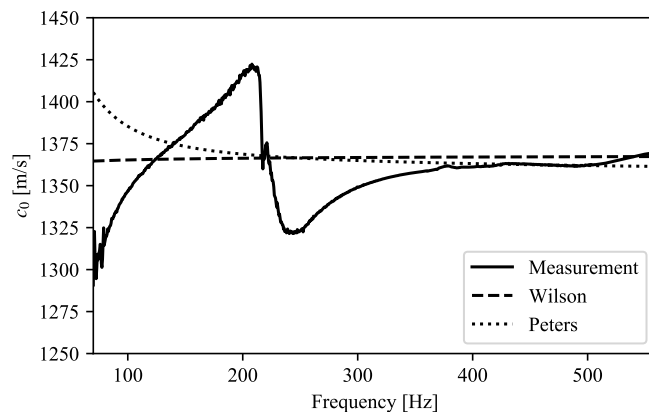
#### 4. Porous material absorption properties

The validated impedance tube was used to measure the absorption of an open-cell metal foam. Three metal-foam samples with about the same porosity (over 90 %) and three different pore sizes were tested, labelling them foam A, foam B and foam C. More detailed properties are given in Tab. 2. Their porous structure is shown in Fig. 10.

Measurements were conducted according to the two-load standard method [9]. In this way any assumption of sample symmetry was avoided. The samples were



(a)



(b)

Figure 8: Complex wavenumber components obtained with different methods, Wilson: analytical equation [5], Peters: broadband spectroscopy method [17], Measurement: amplitude-matching method ( $A = C$  and  $B = D$ ); a) Attenuation coefficient, b) Phase sound velocity.

impregnated with transformer oil to avoid any air bubbles and inserted into the middle of the tube. There they were clamped down through the tube wall with sealed screws.

## 5. Results and discussion

Based on the measurements without foam, the reflection coefficient of termination can be calculated by comparing the reflected and incident waves at the termination location  $x_t$  (Fig. 1):

$$r = \frac{D}{C} e^{2jkx_t}. \quad (30)$$

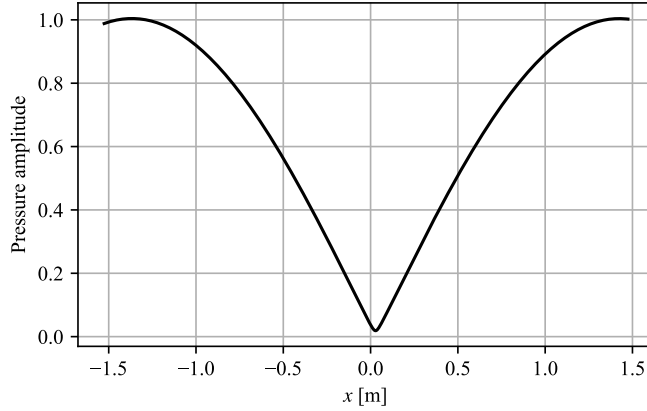


Figure 9: Pressure distribution along the x-axis of the tube at 216 Hz. It should be noted that the coordinate system's origin does not coincide with tube's center.

Table 2: Characteristics of metal-foam samples. Samples have a thickness of 30 mm and a diameter of 79 mm.

Label	Pore size
A	1,4 mm (20 PPI)
B	0,8 mm (30 PPI)
C	0,4 mm (60 PPI)

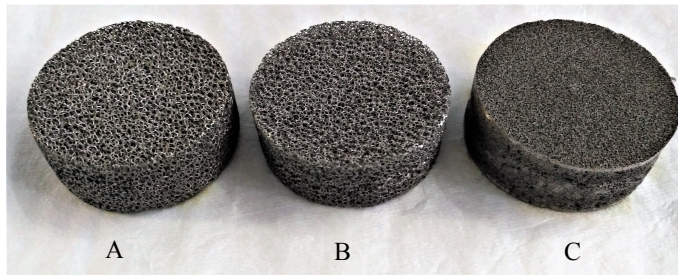


Figure 10: Metal-foam samples and corresponding labels.

As can be seen in Fig. 11 the termination configuration  $\delta = 0$  is close to being acoustically rigid, but not completely. The measurement with the decompression slot shows the effective dissipation around a frequency of 200 Hz, and the difference between the two loads becomes smaller with higher frequency. As reported by Salissou and Panneton [13] more accurate results are achieved with the combination of two loads that have distinctively different reflection properties. The best combination would be a combination of a rigid and an anechoic termination. No such boundary conditions could be provided, since they are not feasible in a liquid medium. However, Salissou and Panneton [13] obtained

steady results with combination of a rigid and an absorbent termination in the frequency range where corresponding reflection coefficients differed for more than 10%. Such condition is also met with our terminations (Fig. 11).

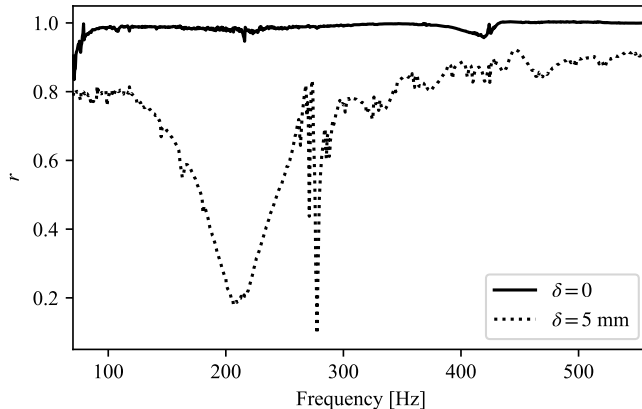
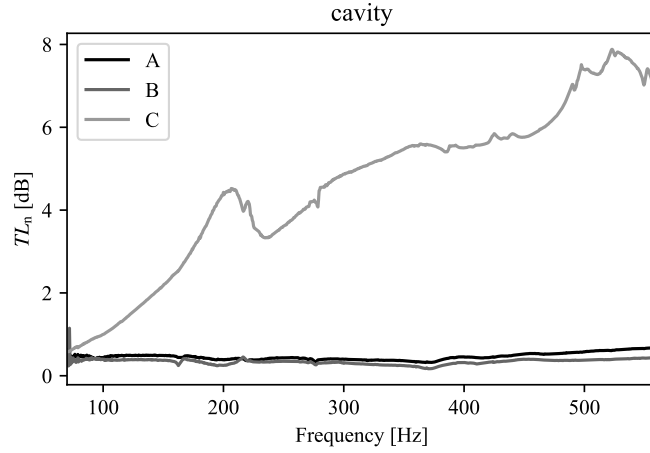


Figure 11: Reflection coefficient of the tube’s termination for each acoustic load,  $\delta = 0$ : decompression slot closed,  $\delta = 5$  mm: decompression slot open.

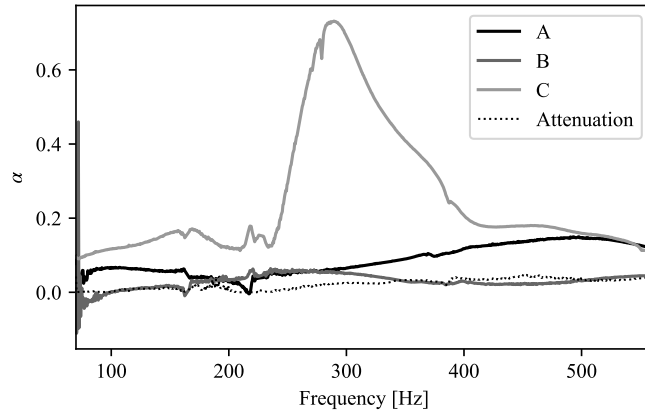
Then, following the standard procedure, the measurements with the metal-foam samples were conducted. The transmission loss and the absorption coefficient were calculated with the new formulation for the cavity-backed configuration. The results for all the samples are compared in Fig. 12. Contrary to expectations, foam A has better absorption than foam B. Foam C provides multiple times higher transmission losses than both foam A and foam B, which can be associated with larger surface in contact with fluid and corresponding viscous and thermal dissipation. On the contrary, foam C does not exhibit such superior absorption coefficient, which indicates that major part of incident wave gets reflected due to the small pores and the high pore density. The exception is frequency range in vicinity of 300 Hz, where mode shape imposes highest pressure at location of the foam. This maximises part of incident wave that is transmitted through the foam and subjected to the transmission losses. A plot of the absorption due to the attenuation is added in Fig. 12b.

Effects of different types of the terminations on  $\alpha$ , obtained with Eq. (11), (13) and (15), are presented on Fig. 13. Absorption of both cavity backed sample and sample in the tube with anechoic termination is heavily dependent on the frequency and the tube’s pressure mode that frequency corresponds to. On the contrary, rigid termination does not cause such fluctuations since foam is always positioned at the pressure maximum.

Discussed results were obtained according to the two-load method, which requires measurements with two different boundary conditions. Each separate boundary condition can also be examined with one-load method [9] under assumption of symmetry and reciprocity of the transfer matrix. On Fig. 14 the two-load method is compared to the one-load method for the tube with



(a)



(b)

Figure 12: Measured dissipation in samples for the case of cavity-backed samples; a) Transmission loss, b) Absorption coefficient.

and without decompression slot. Similar results are obtained with all methods. Highest transmission loss is generated by one-load method with decompression slot ( $\delta = 5$  mm). Without decompression slot  $TL_n$  reaches lowest values and experiences sudden dip at 237 Hz. Two-load method produces the most steady results and predominantly fits in between the one-load method lines.

## 6. Conclusions

The implementation of a low-frequency impedance tube in a liquid medium was investigated. The transfer-matrix method was chosen for the absorption

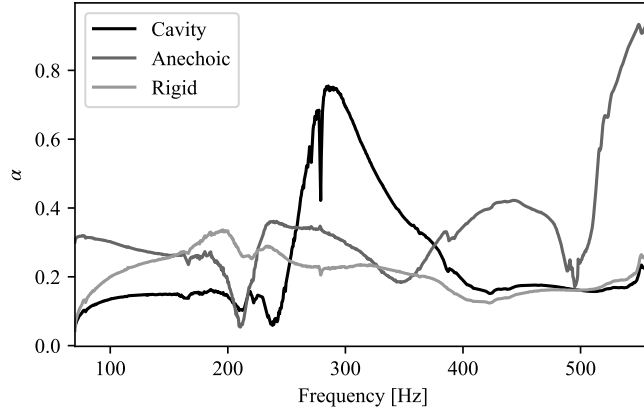


Figure 13: Absorption dependency on the tube's termination for foam C.

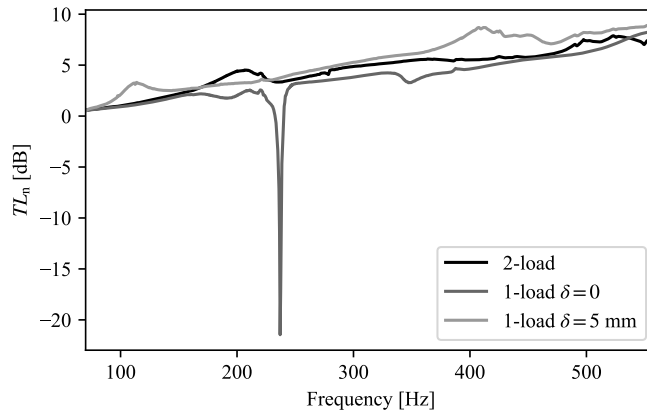


Figure 14: Comparison of two-load method and one-load method for foam C in the cavity-backed configuration.  $\delta$  indicates type of tube's termination.

measurement technique due to the reported low absorption of porous materials in the low-frequency range and the general applicability of the transfer matrix itself. The corresponding tube design requires a cavity-backed configuration of the sample positioning. As the ASTM E2611 standard's recommendations do not account for all phenomena in underwater acoustics, a new instrument for use in liquid media was developed and validated in transformer oil. Specifically for cavity-backed configuration measurements' analysis a new set of equations for reflection and transmission coefficients was also derived, combining the formulations of the transfer matrix and the scattering matrix.

The impedance tube's validation process consists of sound-velocity measurements, waveguide-effect investigations and tube-attenuation determinations.

Since the group velocity of transformer oil is not generally known, a set of methods applicable to the impedance tube were tested. Two of them, i.e., the method of natural modes and the cross-correlation method, are introduced in this paper. The results show that the most reliable group velocity calculation is cross-correlation, but only when the appropriate lengths of the time signals are provided, i.e., without any reflection. The natural modes method should also be a good fit, but would require the use of a different length correction  $l'$  for a finite size flange, as the method gives a higher value of the velocity than expected.

Employing the measured group velocity, a waveguide-effects analysis was conducted, where axi-symmetric modes of the elastic tube were taken into account. Finding two modes, ET0 and ET1, present in the frequency range of interest, it was shown that a loudspeaker with a spherical wave propagation does not excite the mode ET1 and is therefore appropriate for plane-wave excitation in the low-frequency range.

The impedance-tube design with a four-point measuring system is also convenient for phase-velocity and tube-attenuation measurements. As the established methods for complex-wavenumber measurements did not produce accurate results, a new method of amplitude matching was developed. Any assumptions about an absolutely rigid termination were avoided, since such a boundary condition is very difficult to achieve in a liquid environment, as the measurements showed. A mismatch between the analytical and numerical methods was observed, confirming that the pivotal acoustic parameters of the liquid media should be determined on-site.

Finally, with the validated impedance tube, measurements of the metal foam's absorption in transformer oil were conducted. It was observed that absorption properties of the samples exhibit heavy dependence on pressure mode in cavity backed and anechoic configuration. This explains the importance of proper position of the absorption material in low frequency range. Comparison between one-load and two-load method showed that one-load assumptions cause local deviations.

## References

- [1] X. Wang, Porous metal absorbers for underwater sound, *J. Acoust. Soc. Am.* 122 (2007) 2626–2635. doi:10.1121/1.2785041.
- [2] L. Sun, H. Hou, Measurement of sound absorption by underwater acoustic material using pulse-separation method, *Applied Acoustics* 85 (2014) 106–110. doi:10.1016/j.apacoust.2014.04.009.
- [3] W. Xu, C. Jiang, J. Zhang, Underwater acoustic absorption of air-saturated open-celled siliconcarbide foam, *Colloids and Surfaces A: Physicochem. Eng. Aspects* 471 (2015) 153–158. doi:10.1016/j.colsurfa.2015.01.091.

- [4] W. Xu, C. Jiang, J. Zhang, Improvement in underwater acoustic absorption performance of open-celled SiC foam, *Colloids and Surfaces A: Physico-chem. Eng. Aspects* 482 (2015) 568–574. doi:10.1016/j.colsurfa.2015.06.046.
- [5] P. S. Wilson, R. A. Roy, W. M. Carey, An improved water-filled impedance tube, *J. Acoust. Soc. Am.* 113 (2003) 3245–3252. doi:10.1121/1.1572140.
- [6] ASTM E1050–12, Standard test method for impedance and absorption of acoustical materials using a tube, two microphones and a digital frequency analysis system, ASTM Committee, 2012.
- [7] F. Han, G. Seiffert, Y. Zhao, B. Gibbs, Acoustic absorption behaviour of an open-celled aluminium foam, *Journal of Physics D: Applied Physics*. 36 (2003) 294–302. doi:10.1088/0022-3727/36/3/312.
- [8] M. A. Navacerrada, P. Fernández, C. Díaz, A. Pedrero, Thermal and acoustic properties of aluminium foams manufactured by the infiltration process, *Applied Acoustics* 74 (2013) 496–501. doi:10.1016/j.apacoust.2012.10.006.
- [9] ASTM E2611–09, Standard test method for measurement of normal incidence sound transmission of acoustical materials based on the transfer matrix method, ASTM Committee, 2009.
- [10] B. H. Song, J. S. Bolton, A transfer-matrix approach for estimating the characteristic impedance and wave numbers of limp and rigid porous materials, *J. Acoust. Soc. Am.* 107 (2000) 1131–1152. doi:10.1121/1.428404.
- [11] M. Åbom, Measurement of the scattering-matrix of acoustical two-ports, *Mechanical Systems and Signal Processing* 5 (1991) 89–104. doi:10.1016/0888-3270(91)90017-Y.
- [12] L. Feng, Modified impedance tube measurements and energy dissipation inside absorptive materials, *Applied Acoustics* 74 (2013) 1480–1485. doi:10.1016/j.apacoust.2013.06.013.
- [13] Y. Salissou, R. Panneton, A general wave decomposition formula for the measurement of normal incidence sound transmission loss in impedance tube, *J. Acoust. Soc. Am.* 125 (2009) 2083–2090. doi:10.1121/1.3081504.
- [14] K. M. Ho, Z. Yang, X. X. Zhang, P. Sheng, Measurements of sound transmission through panels of locally resonant materials between impedance tubes, *Applied Acoustics* 66 (2005) 751–765. doi:10.1016/j.apacoust.2004.11.005.
- [15] P. Bonfiglio, F. Pompili, A single measurement approach for the determination of the normal incidence transmission loss, *J. Acoust. Soc. Am.* 124 (2008) 1577–1583. doi:10.1121/1.2951605.

- [16] W. Wang, P. J. Thomas, T. Wang, A frequency-response-based method of sound velocity measurement in an impedance tube, *Meas. Sci. Technol.* 28 (2017) 1–8. doi:10.1088/1361-6501/aa5ae0.
- [17] F. Peters, L. Petit, A broad band spectroscopy method for ultrasound wave velocity and attenuation measurement in dispersive media, *Ultrasonics* 141 (2003) 357–363. doi:10.1016/S0041-624X(03)00109-4.
- [18] K. Hou, J. S. Bolton, A transfer matrix method for estimating the dispersion and attenuation of plane waves in a standing wave tube, *J. Acoust. Soc. Am.* 125 (2009) . doi:10.1121/1.4808751.
- [19] J. Han, D. W. Herrin, A. F. Seybert, Accurate measurement of small absorption coefficients, *SAE Technical Paper 2* (2007) . doi:10.4271/2007-01-2224.
- [20] H. Bodén, M. Åbom, Influence of errors on the two-microphone method for measuring acoustic properties in ducts, *J. Acoust. Soc. Am.* 79 (1986) 541–549. doi:10.1121/1.393542.
- [21] C. Peng, D. Morrey, P. Sanders, The measurement of low frequency impedance using an impedance tube, *Journal of Low Frequency Noise, Vibration and Active Control* 17 (1998) 1–10. doi:10.1177/026309239801700101.
- [22] V. A. Del Grosso, Analysis of multimode acoustic propagation in liquid cylinders with realistic boundary conditions – application to sound speed and absorption measurements, *Acta Acustica united with Acustica* 24 (1971) 1435–1445.
- [23] K. Baik, J. Jiang, T. G. Leighton, Acoustic attenuation, phase and group velocities in liquid-filled pipes: Theory, experiment, and examples of water and mercury, *J. Acoust. Soc. Am.* 128 (2010) 2610–2624. doi:10.1121/1.3495943.
- [24] F. Silva, P. Guillemain, J. Kergomard, B. Mallaroni, A. N. Norris, Approximation formulae for the acoustic radiation impedance of a cylindrical pipe, *Journal of Sound and Vibration* 322 (2009) 255–263. doi:10.1016/j.jsv.2008.11.008.
- [25] N. Ogawa, F. Kaneko, Open end correction for a flanged circular tube using the diffusion process, *Eur. J. Phys.* 34 (2013) 1159–1165. doi:10.1088/0143-0807/34/5/1159.
- [26] B. F. G. Katz, Method to resolve microphone and sample location errors in the two-microphone duct measurement method, *J. Acoust. Soc. Am.* 108 (2000) 2231–2237. doi:10.1121/1.1314318.
- [27] L. D. Lafleur, F. D. Shields, Low-frequency propagation modes in a liquid-filled elastic tube waveguide, *J. Acoust. Soc. Am.* 97 (1995) 1435–1445. doi:10.1121/1.412981.

- [28] M. Yang, G. Ma, Z. Yang, P. Sheng, Coupled membranes with doubly negative mass density and bulk modulus, *Phys. Rev. Lett.* 110 (2013) 751–765. doi:10.1103/PhysRevLett.110.134301.